Numerical Analysis of Deterministic Switching of a Perpendicularly Magnetized Spin-Orbit Torque Memory Cell

**R. L. DE ORIO [1], J. ENDER [2], S. FIORENTINI [2], W. GOES[3],
S. SELBERHERR [1] (Life Fellow, IEEE), AND V. SVERDLOV [2]**

1 Institute for Microelectronics, TU Wien, 1040 Vienna, Austria
2 Christian Doppler Laboratory for Nonvolatile Magnetoresistive Memory and Logic, Institute for Microelectronics, TU Wien, 1040 Vienna, Austria
3 Silvaco Europe Ltd., Cambridge PE27 5JL, U.K.

CORRESPONDING AUTHOR: R. L. de ORIO (e-mail: orio@iue.tuwien.ac.at)

ABSTRACT We propose a magnetic field-free spin-orbit torque switching scheme based on two orthogonal current pulses, for which deterministic switching is demonstrated via numerical simulations. The first current pulse selects the cell, while the second current pulse ensures deterministic switching of the selected cell. 100% switching probability has been obtained for a wide range of amplitudes and durations of the pulses, thus precise timings are not required. This has also been verified considering a variability of ±5% of the saturation magnetization and anisotropy constant. An important feature of the scheme is that the magnitude of the second current is lower than the critical current for spin-orbit torque switching. The lower second current pulse improves the efficiency of the switching, reducing the corresponding pulse power by 75% and the total writing power by 40%, while maintaining the same switching time. Due to the sub-critical current, the corresponding spin-orbit torque is weak and does not disturb the bits of non-selected cells. Therefore, a single additional wire can be routed through several cells in a row, reducing the number of transistors per cell, and simplifying the cell integration in a memory array.

INDEX TERMS Spin-orbit torque MRAM, perpendicular magnetization, magnetic field-free switching, two-pulse switching scheme.

I. INTRODUCTION

Spin-orbit torque (SOT) magnetoresistive random access memory (MRAM) is a promising future nonvolatile memory solution for ultra-fast operation beyond the spin-transfer torque MRAM. In particular, it is a viable candidate for a nonvolatile replacement of high-level caches, as it delivers high operation speed and large endurance [1]. However, for deterministic SOT switching of a perpendicularly magnetized free layer (FL) an external magnetic field is required [2], which is cumbersome for large scale integration. In order to circumvent this issue, several field-free schemes have been proposed [3], [4], [5], [6].

Recently, Garello *et al.* [7], [8] demonstrated a successful integration of a cobalt nanomagnet which provides the required magnetic field for deterministic switching of the

SOT cell. In turn, Honjo *et al.* [9] showed the integration of a canted SOT cell, for which the shape of the cell and its orientation with respect to the applied current direction is controlled, but for an in-plane magnetized FL.

An alternative field-free scheme is based on purely electrical switching using two orthogonal current pulses [10]. In this scheme a second heavy metal layer is grown on top of the FL, but with the advantage that no modification of the layers or of the fabrication processes is required. It was shown that this scheme is suitable for switching of a rectangular and of a square FL, and the physical mechanism of the magnetization reversal was clarified [11]. In order to perform switching, the current densities of both pulses were larger than the critical value for SOT switching. This not only yields a fairly high power consumption, but also

complicates the integration of the cell in a memory array, because the additional heavy metal wire conducting such a large current cannot be connected to several cells in a row.

In this work we show that decreasing the current density of the second pulse below the critical value considerably supports the cell integration and reduces its power consumption. After a selection of the cell by the first current pulse, the current of the second pulse can be reduced to 50% of the critical value, while still guaranteeing deterministic and very fast switching of a perpendicularly magnetized FL. The scheme becomes more efficient, because the lower current leads to a reduced writing power for the same switching performance. In addition, the cell integration in a cross-bar architecture becomes simpler, as the second current can be applied to a single heavy metal line connected to several cells in an array without disturbing the information of non-selected cells.

II. SOT CELL SWITCHING

The memory cell and the switching scheme are shown in Fig. 1(a). In this cell the writing and reading paths are decoupled. The SOT-writing part of the cell is formed by a perpendicularly magnetized FL on top of a heavy metal wire (NM1) and a second, orthogonal heavy metal wire (NM2). The magnetic orientation of the FL is read through the tunneling magnetoresistance of a magnetic tunnel junction grown on top. Since the MTJ lies next to the NM2 wire, the latter contacts only part of the FL.

The FL magnetization is flipped electrically, i.e., without an external magnetic field, by a sequence of current pulses. Fig. 1(b) shows a schematic of the switching mechanism. A first current pulse is applied to the NM1 wire, which selects the cell to be written and puts the magnetization in the plane of the FL pointing to the y direction (red arrow). Upon the application of the second pulse, the magnetization of the FL under the NM2 wire, which overlaps just part of the FL, is rotated towards the $-x$ axis (blue arrow). The resulting magnetization configuration creates an in-plane dipolar magnetic field which acts on the rest of the FL. This field generates a torque on the magnetization to complete the switching deterministically, similar to an applied external field. It should be pointed out that the effective field creation is the result of a dynamic process driven by two consecutively applied current pulses. Two simultaneously applied pulses cannot determine the switching [12].

The above mechanism allows bipolar switching. The first current pulse puts the magnetization in the FL plane and the final magnetization state is independent of the current pulse direction. The final magnetization configuration is determined by the polarity of the second current pulse, which deterministically drives the magnetization up or down.

Fig. 1(c) depicts the integration of SOT cells for the two-pulse switching scheme as a cross-bar architecture of a memory array circuit. The writing operation starts with the application of the first current pulse, which flows through the bitline (BL), the heavy metal wire 1 (NM1), and the write source line 1 (WSL1), when the access transistor of
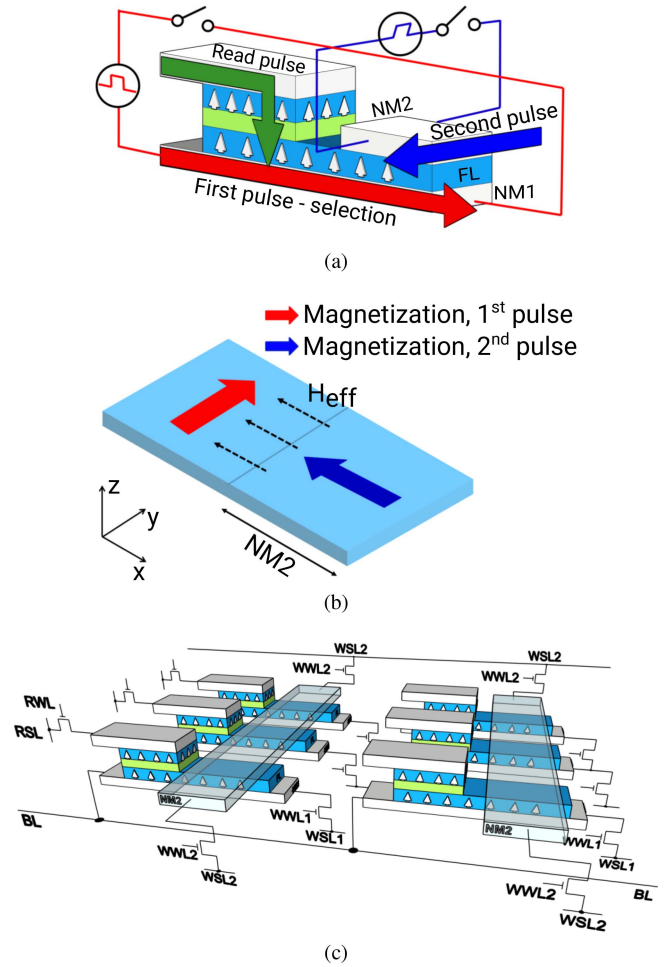
FIGURE 1. (a) SOT switching of a FL by two orthogonal current pulses. (b) Schematic of the two-pulse switching mechanism. (c) Cross-bar architecture depicting the connection of the memory array cells via the NM1 and NM2 wires.

the cell is activated by the word write line 1 (WWL1) signal. Then, the second current pulse is applied through the write source lines 2 (WSL2) and the second heavy metal wire (NM2 routed through several cells in an array), when the access transistors are enabled by the word write lines 2 (WWL2) signal, and the switching of the cell is completed. The read operation is carried out by activating the read word line (RWL) and sensing the tunneling magnetoresistance of the MTJ with the current applied at the read source line (RSL).
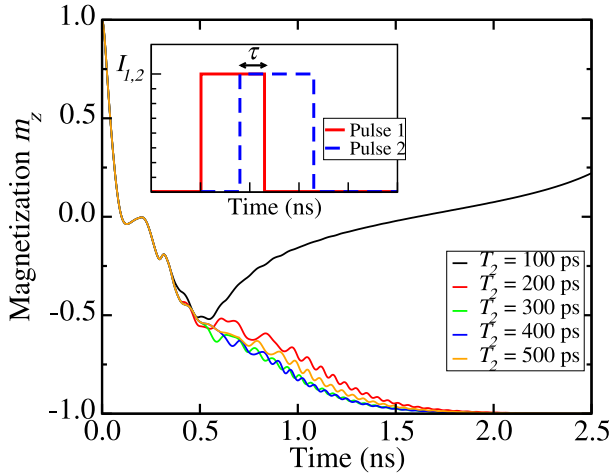
The magnetization dynamics of the magnetic system is described by the Landau-Lifshitz-Gilbert equation complemented with the SOT term.

$$\frac{\partial \mathbf{m}}{\partial t} = -\gamma \mu_0 \mathbf{m} \times \mathbf{H}_{\text{eff}} + \alpha \mathbf{m} \times \frac{\partial \mathbf{m}}{\partial t}$$
$$- \gamma \frac{\hbar}{2e} \frac{\theta_{SH} j}{M_S d} [\mathbf{m} \times (\mathbf{m} \times \mathbf{s})] \qquad (1)$$

$\mathbf{m}$ is the normalized magnetization, γ is the gyromagnetic ratio, μ_0 is the vacuum permeability, α is the Gilbert damping factor, j is the applied current density, and $\mathbf{s}$ is the spin

TABLE 1. Parameters used in the simulations. Heavy metal wires are assumed to be β-tungsten and the magnetic FL to be CoFeB on MgO [2].

Saturation magnetization, M_S	1.1×10^6 A/m
Exchange constant, A	1.0×10^{-11} J/m
Perpendicular anisotropy, K	8.4×10^5 J/m^3
Gilbert damping factor, α	0.035
Spin Hall angle, θ_{SH}	0.3
Free layer dimensions	40 nm $\times$ 20 nm $\times$ 1.2 nm
NM1, NM2: $w_{1,2} \times l$	20 nm $\times$ 3 nm

FIGURE 2. Magnetization switching dynamics for various second pulse durations. Inset: schematic of the two-pulse configuration. The simulation parameters are $I_1 = 160\,\mu$A, $I_2 = 80\,\mu$A, $T_1 = 200$ ps, and $\tau = 0$.

(a)

(b)

FIGURE 3. Contour plot of the switching probability (70 realizations) (a) as a function of both pulse widths and (b) as a function of the second current and pulse width.
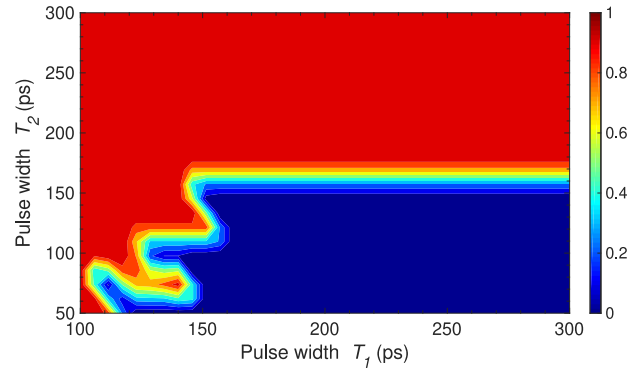
polarization direction. $\mathbf{H}_{\text{eff}}$ includes the exchange field, uniaxial perpendicular anisotropy field, demagnetization field, current-induced field, and random thermal field at 300 K.

In (1) only the damping-like torque (DLT) is considered. It has been shown that a large field-like torque (FLT) can be generated depending on the heavy metal thickness and contribute to symmetry breaking for deterministic SOT switching, affecting the switching characteristics and dynamics [13], [14], [15]. However, the magnitude and direction of the FLT/DLT ratio is still not entirely clear [16]. Large FLT has been reported for Ta-based SOT structures [8], [14], while for W-based structures a much smaller FLT is normally observed [8], [17], up to one order of magnitude lower than the DLT [17]. In this work, we assume SOT cells based on β-tungsten heavy metal wires and neglect the FLT.
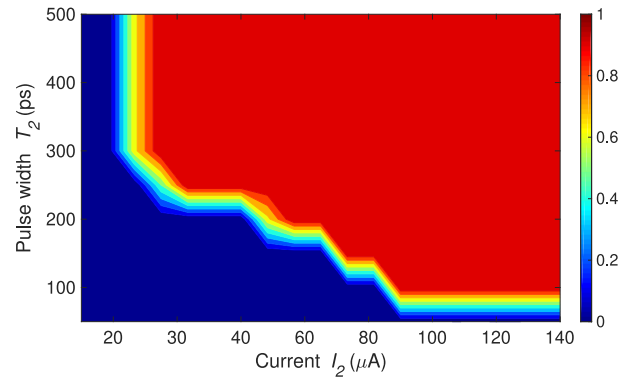
Equation (1) is solved numerically using the finite difference method implemented in an in-house micromagnetic simulation tool (ViennaMag) [18], [19]. The parameters of the FL are listed in Table 1. The thermal stability factor of the cell is 45 and the critical current is $I_c = 120\,\mu$A, which corresponds to a critical current density of $j_c = 2.0 \times 10^{12}$ A/m^2, consistent with [2].

III. RESULTS AND DISCUSSION

Fig. 2 shows the switching dynamics of the SOT cell resulting from the two-pulse scheme. The first pulse, applied to NM1, selects the cell with a current $I_1 = 160\,\mu$A

($j_1 = 2.67 \times 10^{12}$ A/m^2) and a fixed duration $T_1 = 200$ ps. Then, the second current pulse is applied with $I_2 = 80\,\mu$A ($j_2 = 1.33 \times 10^{12}$ A/m^2) and various pulse durations are considered, as shown in Fig. 2. Each curve corresponds to the average of 70 realizations, due to the stochastic thermal field. Here, deterministic switching is obtained for the longer pulse durations (≥ 200 ps) and the switching dynamics are very similar for these cases.

In order to evaluate the operation window of the scheme, the pulse parameters are varied and the switching probability is determined. Fig. 3(a) shows a contour plot of the switching probability (70 stochastic simulations) as function of both pulse widths. Here, $I_1 = 160\,\mu$A and $I_2 = 80\,\mu$A, the latter being lower than the critical current. When both pulses are short (≤ 150 ps), the switching strongly depends on the precise timing of the pulses, which makes it unreliable, since small variations to the pulses' timing already lead to non-deterministic switching. In addition, if T_1 is increased (> 150 ps), while T_2 remains short, no switching is observed.

This unreliable switching can be circumvented by applying a longer second pulse. For $T_2 \geq 200$ ps the switching becomes deterministic for all used T_1 values. 100% switching is obtained for a wide range of pulse durations, thus precise timings are not required. In addition, increasing the pulse
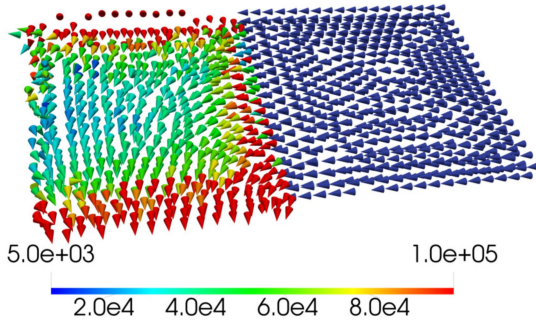
FIGURE 4. Dipolar field created by the two-pulse scheme in the FL. The blue arrows on the right represent the magnetization under the NM2 wire. On the left, the color-coded arrows represent the generated magnetic field (in A/m).

FIGURE 5. Switching realizations for various delays/overlaps between the pulses. $\tau < 0$ represents an overlap while $\tau > 0$ represents a delay between the first and the second pulse (inset of Fig. 2). The simulations are carried out for $I_1 = 160\ \mu A$, $I_2 = 80\ \mu A$, $T_1 = T_2 = 200\ ps$.

duration has a relevant impact on the required current amplitude for deterministic switching, i.e., longer pulse durations allow a reduction of the applied current. Fig. 3(b) shows the switching probability as a function of the second current pulse amplitude and duration. For a operation window below 500 ps, a minimum current of 30 µA is required, which is four times lower than the nominal critical current. Another solution to ensure deterministic switching is to increase the second current which, in turn, allows shorter T_2, as reported in Fig. 3(b). For I_2 about 110 µA, 100% switching is already observed for T_2 as short as 100 ps.

Since I_2 is low in, see Fig. 3(a), when T_2 is small (≤ 150 ps), the second pulse is too short to properly orient the magnetization under the NM2 wire and create an in-plane magnetic field to reliably drive the magnetization reversal. The switching is in a "precessional"-like regime, which strongly depends on the magnetization dynamics triggered by the first and second pulse. Thus, the switching is very dependent on precise combinations of T_1 and T_2, in such a way that small variations change the switching behavior. We are interested in deterministic switching and should therefore avoid this region. On the other hand, a sufficiently long T_2 (≥ 200 ps) and/or strong I_2 pulse will rotate the magnetization of the part of the FL under the NM2 wire, as shown by the blue arrows on the right in Fig. 4. This magnetization creates an in-plane dipolar field which acts on the non-overlapped part of the FL, shown on the left in Fig. 4. The x-component of this field averages to about 35 mT, which is similar to that reported in [2] and [7]. In this case, the magnetization of the remaining free part of the FL will precess and be oriented perpendicularly in the wanted direction, dragging along the rest of the FL magnetization, when I_2 is turned off. Therefore, the switching becomes deterministic and does not depend on T_1 in the simulated range. For a higher current, the generated SOT is larger and the magnetization is quickly rotated, consequently a shorter pulse duration is needed. On the other hand, for a lower current, and thus smaller SOT, a longer pulse is required to put the magnetization to the proper orientation.

In order to further investigate the switching probability, we have carried out 5000 stochastic simulations considering
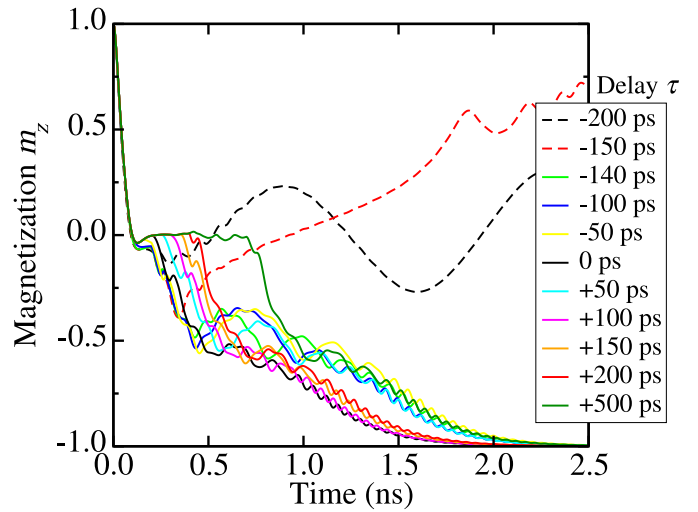
$I_2 = 80$ µA and pulse durations of 200 ps. In this case, 100% switching has been obtained, which confirms that the scheme leads to deterministic switching.

The interconnect structure of practical circuits is a source of signal propagation delay, which results in a delay or in an overlap between the first and the second current pulse. Fig. 5 reports switching realizations for various delays/overlaps (τ) between the pulses, considering $I_1 = 160$ µA, $I_2 = 80$ µA, $T_1 = T_2 = 200$ ps. 100% switching probability is observed up to an overlap of 150 ps, i.e., for longer overlaps the switching is not deterministic anymore. It should be pointed out that 150 ps of overlap represents a large portion of the pulses (75%).

When considering the effect of pulse delays, the switching remains deterministic for very long delays between the pulses. Even for a delay of 500 ps, which corresponds to 2.5 times the pulses' durations, the switching is still reliable. The magnetization dynamics work as follows: the strong first pulse puts the magnetization in the FL plane. While the second pulse is not applied, the magnetization starts to precess and slowly points out of the FL, up and down, due to the stochastic thermal field. In this case, the average m_z-component of the magnetization is close to zero, and this behavior persists until the second pulse is applied and the generated SOT redirects the magnetization under the NM2 wire.

It should be pointed out, however, that it is disadvantageous to operate with long pulse delays, because the time for the magnetization to equilibrate increases and the operation frequency decreases. The robustness of the scheme against relatively long delay/overlap between the pulses indicates that small variations of the pulses' parameters do not impair the determinacy of the cell switching.
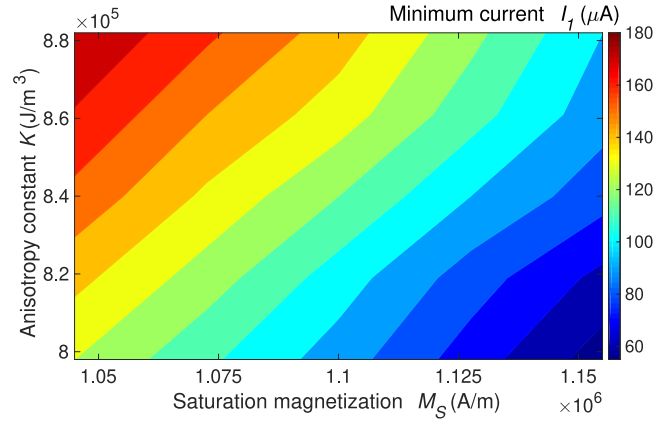
Although the two-pulse scheme requires a larger cell size due to the additional NM2 wire and timing control of two

(a)

(b)
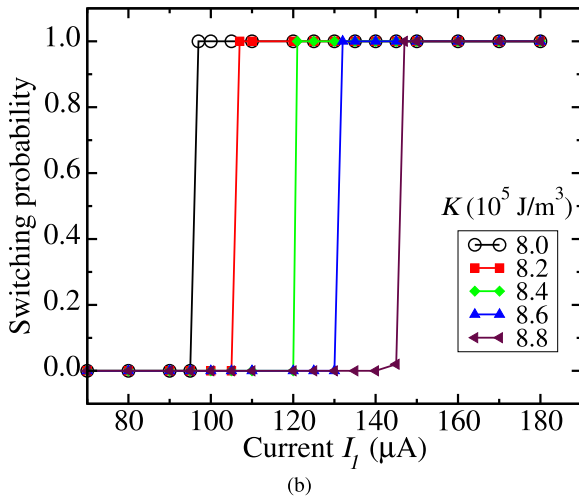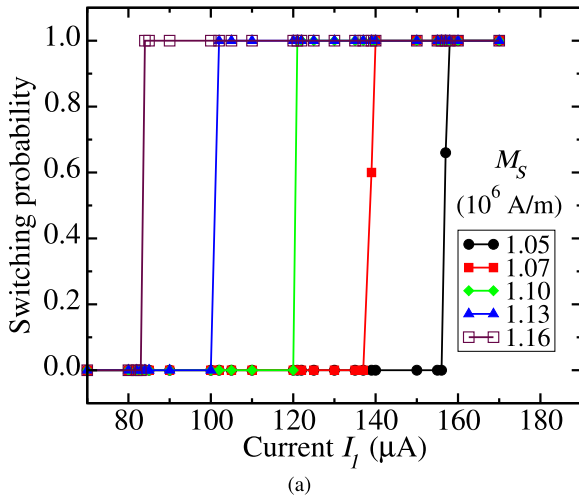
FIGURE 6. Switching probability as a function of I_1 for ±5% variation of the (a) saturation magnetization and (b) of the anisotropy constant relative to the nominal values. Both parameters are varied independently. Each point corresponds to 70 stochastic simulations. The simulations parameters are: I_2 = 80 μA, T_1 = T_2 = 200 ps, and τ = 0.


FIGURE 7. Contour map of the minimum first pulse current to guarantee switching as a function of the saturation magnetization and of the anisotropy constant.

current pulses, it provides a wide design window for the choice of pulse parameters to guarantee deterministic switching. The scheme can thus be optimized, for instance, for switching robustness, energy consumption or endurance.

A critical aspect that has to be taken into account in the design of the two-pulse scheme is the variability of the material parameters from cell to cell, in order to guarantee that deterministic switching is obtained across the whole variation space. Fig. 6 shows the switching probability as a function of the first current pulse amplitude considering a ±5% variation of the saturation magnetization and of the anisotropy constant relative to the nominal values (Table 1), considering that the parameters are varied independently. The variation of the parameters has a direct impact on the critical current density for SOT switching [20]. Thus, by adjusting the first current pulse above the critical current, 100% switching is obtained. Here, a current I_1 = 160 μA

($j_1 = 2.67 \times 10^{12}$ A/m²) yields deterministic switching for the parameter variation reported in Fig. 6.

Fig. 7 shows a contour map of the minimum current for the first pulse required to obtain 100% switching probability, when a simultaneous variation of ±5% is assumed for the saturation magnetization and the anisotropy constant. The ratio of the largest to the lowest required current is rather large, where the lowest current lies at about 60 μA, while the largest current is 180 μA. Thus, by setting I_1 = 180 μA, deterministic switching can be achieved for all possible variations of the material parameters assumed above.

We consider now the four extreme cases of material parameter variation, which are given by the corners of the contour plot of Fig. 7, and analyze the minimum second current pulse amplitude and width which lead to 100% switching probability for the whole material parameter variation range. Fig. 8(a) shows the switching probability as a function of the second pulse amplitude. Although the lowest current which yields switching is 45 μA, the minimum current required for deterministic switching of all parameter combinations is 60 μA. This current is lower than the critical one for almost all parameter combinations. In turn, Fig. 8(b) shows the switching probability as a function of the pulse duration. A pulse as short as 80 ps can yield deterministic switching for some material parameter combinations. However, to guarantee 100% switching for all cases, a minimum pulse width of 150 ps is needed.

An important feature of the scheme is that the magnitude of the second current is lower than the critical current for spin-orbit torque switching. Otherwise, the NM2 wire cannot be routed through various cells in an array as in Fig. 1(c), because the SOT generated by the second current pulse drives the magnetization of the non-selected cells to the FL plane. In this case, not only is the stored information temporarily disturbed, but also the probability of an undesired bit flip increases. For each bit cell an extra access transistor is required to control the current flow through the selected cell only. This increases the number of transistors
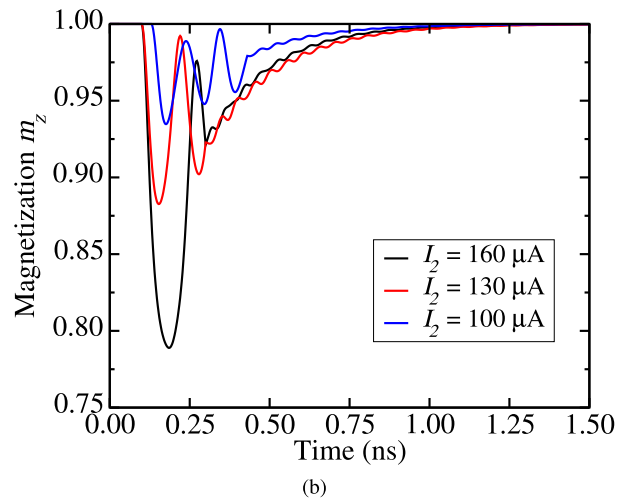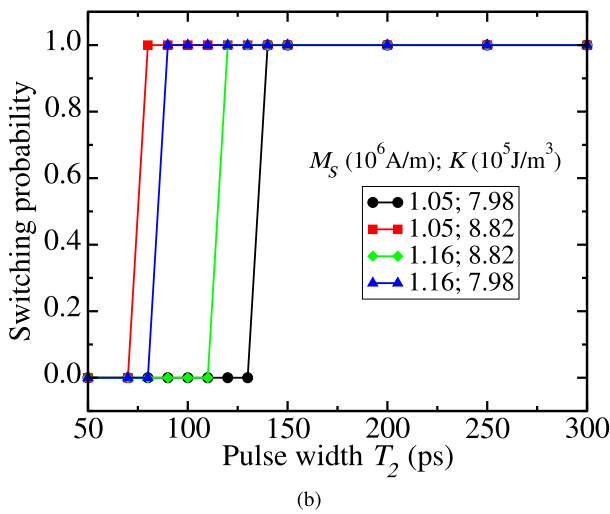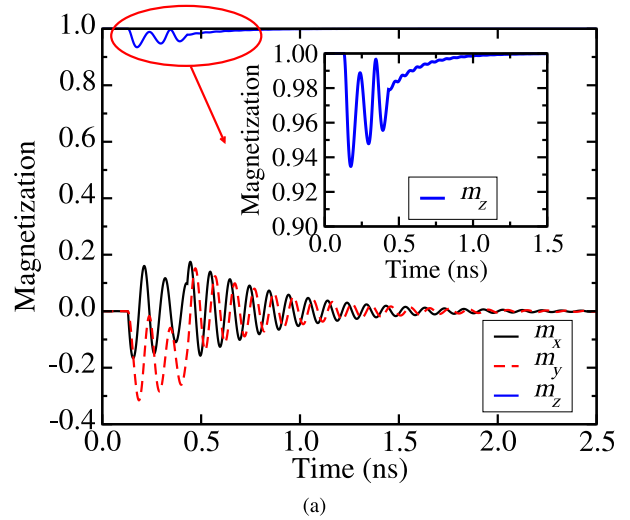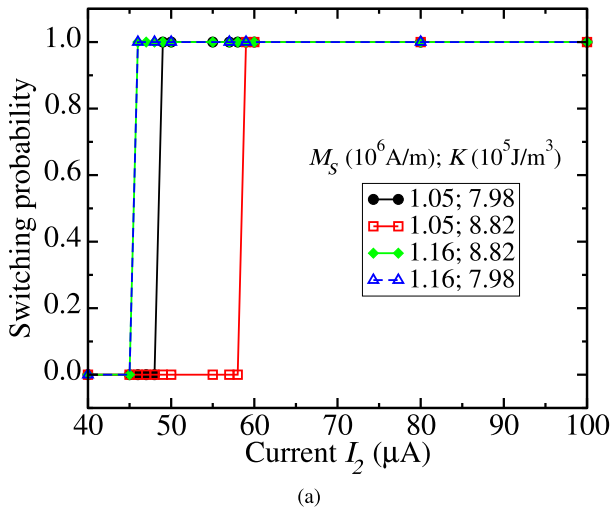
FIGURE 8. Switching probability as a function of (a) the second current pulse and of (b) the pulse width for the four extreme cases of parameter variation (corners of the contour plot of Fig. 7). The simulation parameters are $I_1 = 180\,\mu\text{A}$, $I_2 = 80\,\mu\text{A}$, $T_1 = T_2 = 200$ ps, and $\tau = 0$, unless otherwise stated.

FIGURE 9. Magnetization dynamics without pre-selecting the cell ($I_1 = 0$). (a) Magnetization components for $I_2 = 100\,\mu\text{A}$ (1.7×10^{12} A/m^2). (b) Comparison for different current amplitudes, $T_2 = 200$ ps.

per cell, the cell area, and the wiring overhead, making the cell integration more complex.

For a second current smaller than the critical value, the corresponding SOT is weaker and the non-selected cells should not be disturbed. This is confirmed by the magnetization dynamics shown in Fig. 9(a). Here, the cell is not selected by the first pulse and only the second current pulse is applied. The weak SOT deviates the magnetization from the initial out-of-plane orientation only slightly. The magnetization goes back to its initial position after about 1 ns of the second current pulse. This occurs within the time it takes for the written cell to reach the equilibrium, therefore the operation speed of the array is not expected to be reduced. This proves that the non-selected cells remain undisturbed and an undesired bit flip is unlikely.

Fig. 9(b) shows the magnetization dynamics for different current amplitudes. Here, $I_2 = 100\,\mu\text{A}$ is about 20% lower

than the critical current, while $I_2 = 160\,\mu\text{A}$ is 30% higher. As expected, the higher the current (larger SOT) the larger is the deviation of the magnetization from its initial state. Nevertheless, even for the higher current case this deviation is sufficiently small. Thus, the switching probability tends to zero and an undesired switching is avoided. In addition, since the second heavy metal does not contact the whole FL, the magnetization is deviated in part of the FL only, which makes the switching even less likely. These results indicate that the operation window for the second current pulse yielding 0% switching probability, when the cell is not selected by the first pulse, is very large and its amplitude can be even higher than the critical current.

Importantly, such a large current is not necessary. As previously shown, the second current can be significantly reduced below the critical value. The NM2 wire can be routed through several cells in an array as shown in Fig. 1(c). Consequently, the extra access transistor per cell is not needed, which leads to a smaller cell area and a simpler

cell integration in a memory circuit. Furthermore, the writing current density can be decreased to about 50% of the critical one, while maintaining deterministic switching. It should be noted that decreasing the second current by 50% corresponds to a reduction of 75% of the second pulse's power/energy. In terms of total writing power, when both current pulses are considered ($P \propto (I_1^2 T_1 + I_2^2 T_2)/(T_1 + T_2)$), such a current reduction results in a 40% decrease of the power consumption.

IV. CONCLUSION

We demonstrated via micromagnetic simulations that the two-current pulse switching scheme yields deterministic switching of a perpendicular magnetic free layer by SOTs. The first current pulse amplitude is higher than the critical value to select the cell and puts the magnetization in the plane of the free layer, while the second current pulse completes the switching deterministically. The second current amplitude lower than the critical value can be applied and still guarantee fast and reliable switching. The switching scheme is also robust against small variations of the pulse parameters, including large delays or overlaps between the pulses. By reducing the switching current, a significant decrease in the writing power is obtained and, as a result, the scheme becomes more efficient. In addition, the reduced current does not disturb non-selected cells, thus the second heavy metal wire can be routed through several cells of a memory array, which leads to reduced number of access transistors per cell, and simpler integration. The drawbacks of the scheme are that the additional heavy metal wire increases the cell size and control of the timing of two pulses is required. Nevertheless, the scheme offers a flexible window for designing the pulse parameters for reliable operation with sub-500 ps timings, being promising as a future candidate for embedded MRAM applications.

REFERENCES

[1] A. Manchon and S. Zhang, "Theory of spin torque due to spin-orbit coupling," *Phys. Rev. B, Condens. Matter*, vol. 79, Mar. 2009, Art. no. 094422. [Online]. Available: https://link.aps.org/doi/10.1103/PhysRevB.79.094422

[2] S. Fukami, T. Anekawa, C. Zhang, and H. Ohno, "A spin–orbit torque switching scheme with collinear magnetic easy axis and current configuration," *Nat. Nanotechnol.*, vol. 11, pp. 621–626, Jul. 2016. [Online]. Available: https://doi.org/10.1038/nnano.2016.29

[3] S. Fukami, C. Zhang, S. DuttaGupta, A. Kurenkov, and H. Ohno, "Magnetization switching by spin–orbit torque in an antiferromagnet–ferromagnet bilayer system," *Nat. Mater.*, vol. 15, pp. 535–541, May 2016. [Online]. Available: https://doi.org/10.1038/nmat4566

[4] H. Wu *et al.*, "Spin–orbit torque from a ferromagnetic metal," *Phys. Rev. B, Condens. Matter*, vol. 99, May 2019, Art. no. 184403. [Online]. Available: https://link.aps.org/doi/10.1103/PhysRevB.99.184403

[5] D. MacNeill, G. M. Stiehl, M. H. D. Guimaraes, R. A. Buhrman, J. Park, and D. C. Ralph, "Control of spin–orbit torques through crystal symmetry in WTe2/ferromagnet bilayers," *Nat. Phys.*, vol. 13, pp. 300–305, Mar. 2016. [Online]. Available: https://doi.org/10.1038/nphys3933

[6] G. Yu *et al.*, "Switching of perpendicular magnetization by spin–orbit torques in the absence of external magnetic fields," *Nat. Nanotechnol.*, vol. 9, pp. 548–554, Jul. 2014. [Online]. Available: https://doi.org/10.1038/nnano.2014.94

[7] K. Garello *et al.*, "Manufacturable 300mm platform solution for field-free switching SOT-MRAM," in *Proc. IEEE Symp. VLSI Circuits*, Jun. 2019, pp. T194–T195. [Online]. Available: https://doi.org/10.23919/VLSIC.2019.8778100

[8] K. Garello *et al.*, "SOT-MRAM 300mm integration for low power and ultrafast embedded memories," in *Proc. IEEE Symp. VLSI Circuits*, Jun. 2018, pp. 81–82. [Online]. Available: https://doi.org/10.1109/VLSIC.2018.8502269

[9] H. Honjo *et al.*, "First demonstration of field-free SOT-MRAM with 0.35ns write speed and 70 thermal stability under 400°C thermal tolerance by canted SOT structure and its advanced patterning/SOT channel technology," in *Proc. IEEE Int. Elect. Devices Meeting (IEDM)*, Dec. 2019, pp. 28.5.1–28.5.4. [Online]. Available: https://doi.org/10.1109/IEDM19573.2019.8993443

[10] V. Sverdlov, A. Makarov, and S. Selberherr, "Two-pulse sub-ns switching scheme for advanced spin-orbit torque MRAM," *Solid-State Electron.*, vol. 155, pp. 49–56, May 2019. [Online]. Available: https://doi.org/10.1016/j.sse.2019.03.010

[11] R. L. de Orio *et al.*, "Robust magnetic field-free switching of a perpendicularly magnetized free layer for SOT-MRAM," *Solid-State Electron.*, vol. 168, Jun. 2019, Art. no. 107730. [Online]. Available: https://doi.org/10.1016/j.sse.2019.107730

[12] X. Zhang *et al.*, "Electrical control over perpendicular magnetization switching driven by spin-orbit torques," *Phys. Rev. B, Condens. Matter*, vol. 94, Nov. 2016, Art. no. 174434. [Online]. Available: https://link.aps.org/doi/10.1103/PhysRevB.94.174434

[13] G. Yu *et al.*, "Competing effect of spin–orbit torque terms on perpendicular magnetization switching in structures with multiple inversion asymmetries," *Sci. Rep.*, vol. 6, Apr. 2016, Art. no. 23956. [Online]. Available: https://doi.org/10.1038/srep23956

[14] J. M. Lee *et al.*, "Oscillatory spin–orbit torque switching induced by field-like torques," *Commun. Phys.*, vol. 1, pp. 1–7, Feb. 2018. [Online]. Available: https://doi.org/10.1038/s42005-017-0002-3

[15] C. Kim *et al.*, "Spin–orbit torque driven magnetization switching and precession by manipulating thickness of CoFeB/W heterostructures," *Adv. Electron. Mater.*, vol. 6, no. 2, 2020, Art. no. 1901004. [Online]. Available: https://doi.org/10.1002/aelm.201901004

[16] D. Zhu and W. Zhao, "Threshold current density for perpendicular magnetization switching through spin-orbit torque," *Phys. Rev. Appl.*, vol. 13, Apr. 2020, Art. no. 044078. [Online]. Available: https://link.aps.org/doi/10.1103/PhysRevApplied.13.044078

[17] Y. Takeuchi, C. Zhang, A. Okada, H. Sato, S. Fukami, and H. Ohno, "Spin–orbit torques in high-resistivity-W/CoFeB/MgO," *Appl. Phys. Lett.*, vol. 112, no. 19, May 2018, Art. no. 192408. [Online]. Available: https://doi.org/10.1063/1.5027855

[18] (2016). *ViennaMag.* [Online]. Available: www.iue.tuwien.ac.at/index.php?id=24

[19] A. Makarov, "Modeling of emerging resistive switching based memory cells," Ph.D. dissertation, Inst. Microelectron., TU Wien, Vienna, Austria, 2014. [Online]. Available: www.iue.tuwien.ac.at/phd/makarov/

[20] K.-S. Lee, S.-W. Lee, B.-C. Min, and K.-J. Lee, "Threshold current for switching of a perpendicular magnetic layer induced by spin Hall effect," *Appl. Phys. Lett.*, vol. 102, no. 11, Mar. 2013, Art. no. 112410. [Online]. Available: https://doi.org/10.1063/1.4798288